DC-link Capacitance Estimation based on Discharge Profile of Inverter for EV Application

Xing Wei[1], Yingzhou Peng[2], Bo Yao[1], and Huai Wang[1]
[1] Aalborg University, Denmark
[2] Hunan University, China

***Abstract*-- This paper proposes a non-invasive DC-link capacitance estimation method based on capacitor discharging profile during the turning-off transition of a three-phase inverter. The proposed method relies on existing signals without the need for additional sensors or an upgrade of existing sensors. The presented study aims for Electric Vehicle (EV) traction inverter application due to its frequent parking activities during the use. It minimizes the new risk because the estimation procedure can be implemented after vehicles are parked. The influences of different discharging loading scenarios and constraints in sampling frequency and sensor accuracy are analyzed. The proof-of-concept experiments based on a scaled-down inverter prototype verify the feasibility of the proposed method.**

***Index Terms*-- Electric drive system, DC-link capacitor, discharge, capacitance estimation, condition monitoring.**

I. Introduction

DC-link capacitor is an important part of the electric drive system in electric vehicles (EVs), which can smooth the DC-link voltage variation, absorb the high-frequency harmonics, and balance the instantaneous power difference between the front-end battery and the rear-end load electric machine [1-3].

However, due to the harsh operating and environmental conditions in field applications, the DC-link capacitor is a stand-out component in terms of failure rate in the electric drive system [3-6]. As reported in [7], about 30% of the failures in power electronic converters are caused by the capacitor, and it has been considered one of the most vulnerable components. Hence, it is essential to monitor the operation status and degradation process of the DC-link capacitor to ensure reliable field operation, and consequently, optimal operation and proactive maintenance can be performed before catastrophic failure occurs [7-9].

In the last two decades, much impressive research work has been done on condition monitoring for the capacitor in DC-link applications. Since the physical and electrical characteristics of capacitors change with degradation, several nonelectrical parameters (e.g., structure, weight, internal temperature, internal pressure) and electrical parameters (e.g., capacitance, equivalent series resistance, dissipation factor) have been proposed as health indicators [10]. For the acquisition of nonelectrical parameters, some industrial instruments including weighting meters [11], X-ray image meters [12], thermography meters [13], and internal temperature and pressure sensors [14], etc., are widely employed. However, these measurement instruments are generally expensive, and it is difficult to define uniform end-of-life criteria because the nonelectrical parameters are dependent on the capacitor specifications, such as materials, capacity, rated voltage, etc. In contrast, the electrical parameters are more cost-effective and easy to implement, and it is widely reported that the equivalent series resistance is commonly used to monitor the aluminum electrolytic capacitor, while the capacitance value is applicable for any type of capacitor [15-16]. For applications like electric drive systems where the DC-link is typically designed with film capacitors, capacitance is the preferred health indicator

According to Ohm's law, the capacitor capacitance can be estimated by periodic small-signal ripples, including capacitor voltage ripple and current ripple. In [17], the voltage and current ripples of the DC-link capacitor in an adjustable speed drive (ASD) system are directly measured by sensors, and the Goertzel algorithm is applied to extract the mid-frequency components. To avoid using a capacitor current sensor, M. Makdessi et al. [18] indirectly obtain the capacitor current through the front-end current and rear-end current, but this method requires a measurement system with a wide bandwidth and fast sampling rate. External signal injection methods are proposed in [19]-[22] to estimate the capacitor capacitance in an ASD system. The low-frequency AC current or voltage signal is injected into the front-end ac/dc converter at no-load conditions [19]-[22] or the rear-end dc/ac converter is operated in a regenerative mode [23], and the corresponding induced current or voltage ripple is analyzed by recursive least squares (RLS) algorithm to estimate the capacitance.

Overall, the periodic small-signal ripple-based methods can estimate the capacitance of the DC-link capacitor with relative accuracy. However, they require high-precision sampling, additional hardware, and advanced data processing algorithms, which are costly and complex for field applications. Additionally, most of these methods require the power converter to operate at a specific mode and frequency, which interferes the normal operation.

To avoid normal operation disturbances, several works have been devoted to estimating the capacitor capacitance through the charge and discharge profiles [24]-[29]. For safety reasons, the DC-link capacitor in power electronic converters should be charged and discharged during the

system start-up and shutdown process. In [24]-[26], the DC-link capacitor in the ASD system is discharged through two-phase motor windings when the motor is stopped, and the capacitance is estimated by the small-amplitude capacitor voltage and current ripples. An *LC* resonant circuit formed by the DC-link capacitor and the two-phase motor windings during the discharge process is proposed in [27], and a capacitance estimation model is fitted by the iterative least squares algorithm. However, these schemes need to invade the original software to control the power semiconductor switches with a constant-frequency constant-duty PWM and inevitably induce torque in the load motor due to non-ideal current control. An auxiliary discharge network consisting of switches and resistors is proposed in [28] in parallel with the DC-link capacitor, but the introduced discharge path can bring additional reliability risks. In [29], the three-phase motor windings in EVs are proposed to form the discharge circulation. The DC-link capacitor is discharged with a constant current, and the capacitor capacitance is estimated by the existing information in the controller including the DC-link voltage and three-phase stator currents. However, an additional current control strategy is required to limit the capacitor discharge current and the estimation accuracy is not experimentally verified at different operating and environmental conditions.

In summary, for the capacitance estimation of the DC-link capacitor, there is still a gap between the current academic research and practical implementation. This paper proposes a discharge profile-based capacitance estimation method for the DC-link capacitor in electric drive systems. The DC-link capacitor is discharged through three-phase motor windings with the original current control strategy, and the capacitance is estimated from the existing information in the electric drive system, without software invasion and additional hardware measurement. Moreover, a novel method is proposed to eliminate and compensate for the errors in the existing information caused by measurements and non-ideal switching characteristics. As a result, the estimation accuracy is significantly improved and the requirements for sampling and computation are greatly reduced.

II. Discharge of DC-link Capacitor through Motor Stator Windings

The typical electrical configuration of the electric drive system in EVs is shown in Fig. 1, which consists of the DC-link capacitor, power semiconductor module, electric machine, and control system. The battery is directly connected to the DC-link of the electric drive system through circuit breakers for energy supply, and the electric machine is commonly an AC induction machine or AC permanent magnet type [30].

Film capacitors are widely used for the DC-link design of electric drive systems due to their high ripple current capability, high power density as well as low cost [1]. Fig. 1 gives the simplified model of the DC-link capacitor,

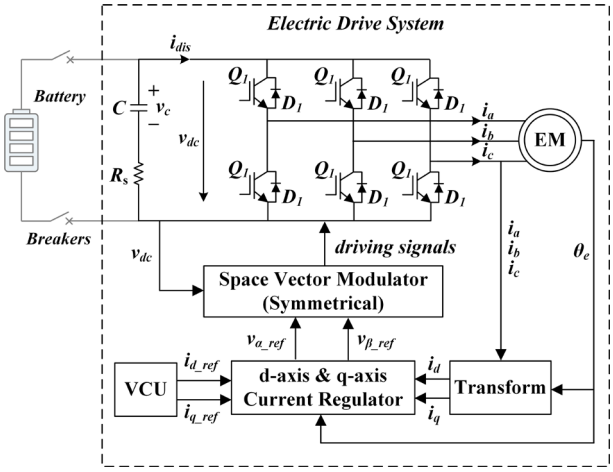

Fig. 1. Electrical configuration of the electric drive system in EVs.

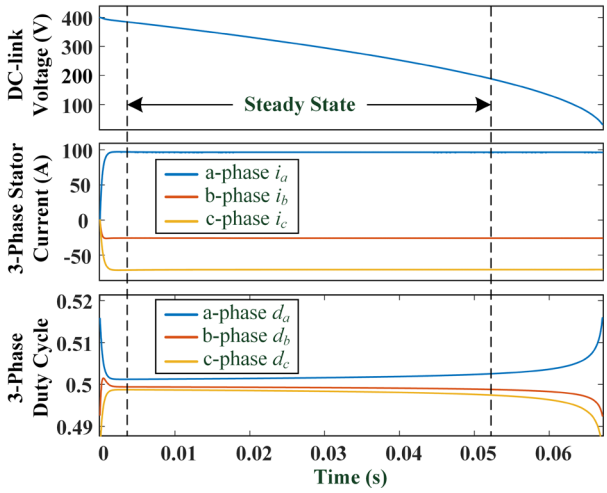

Fig. 2. A typical discharge profile of the DC-link capacitor in electric drive systems with the current reference i_{d_ref} of 100A, initial capacitor voltage of 400V, and rotor electrical angle θ_e of $\pi/12$. $d_a \sim d_c$ are the duty cycles of the three-phase upper switches.

where C and R_s are the capacitance and equivalent series resistance (ESR), respectively. To achieve high operating power, insulated-gate bipolar transistor (IGBT) modules are commonly used in the current EV electric drive system, and $Q_1 \sim Q_6$ and $D_1 \sim D_6$ in Fig. 1 represent the IGBT devices and free-wheeling diodes in the power semiconductor module, respectively. In the future, the automotive power semiconductor module will trend to replace the silicon switches with silicon carbide (SiC) and gallium nitride (GaN) devices to further reduce power loss and system size [6].

For safety reasons, when the vehicle system is shut down, the circuit breakers in Fig. 1 are opened to disconnect the electric drive system from the battery, and the DC-link in the electric drive system has to be discharged. When the vehicle control unit (VCU) monitors that the motor speed is zero and the circuit breakers have been opened, the discharge current commands i_{d_ref} and i_{q_ref} in the rotor flux reference frame are issued, as shown in Fig. 1. The d-axis current reference i_{d_ref} is typically fixed and determined by the discharge time requirement,

while the q-axis current reference i_{q_ref} must be set to null to avoid torque generation. To achieve the closed-loop control and the decoupling in current and back-electromagnetic force, the three-phase stator currents i_a, i_b, and i_c are measured and transformed to the rotor flux reference frame according to the rotor electrical angle θ_e, which is random but fixed within one discharge process. The electric drive system in EV applications is typically modulated by the symmetrical space vector strategy, and the switching sequence is determined by the DC-link voltage v_{dc} and the voltages reference v_{α_ref} and v_{β_ref} in the stationary reference frame provided by the current regulator. As the power semiconductor module is driven, the discharge current i_{dis} flows through the power module and the back-end motor stator windings, and the energy stored in the DC-link capacitor is consumed by the equivalent resistors in the circulation loop.

Fig. 2 gives a typical discharge profile of the DC-link capacitor in the electric drive system with the initial capacitor voltage of 400V, d-axis current reference i_{d_ref} of 100A, and rotor electrical angle θ_e of π/12, in which the analog and digital signals are all existing information in the electric drive system. It can be seen that the three-phase stator currents i_a, i_b, and i_c have fixed polarity in the discharge and reach a steady state after a transient process. The steady-state value of the phase currents are monotonically determined by the rotor electrical angle θ_e due to the fixed discharge current reference i_{d_ref}, and the duty cycles of the upper switches within the steady-state interval are all around 0.5. The current command $i_{\mathrm{d\_ref}}$ begins to decrease after the DC-link voltage v_{dc} falls below a safety voltage.

III. Discharge Profile-based Capacitance Estimation

According to ohm's law, the capacitance C of the DC-link capacitor can be estimated through the capacitor discharge current i_{dis} and the capacitor voltage v_{C} as

$$C = \frac{\int_{t_0}^{t_0+\Delta t} i_{dis}\,dt}{\Delta v_C} \tag{1}$$

where Δt is the estimation interval, and Δv_{C} is the capacitor voltage drop during the estimation interval. Since the capacitor discharge current i_{dis} is always positive, the integral term in (1) can be rewritten as

$$C = \frac{i_{dis\_ave}\Delta t}{\Delta v_C} \tag{2}$$

where $i_{\mathrm{dis\_ave}}$ represents the average capacitor discharge current over the estimation interval.

Fig. 3 gives the key waveforms within the ith switching period t_0 - t_8 of the discharge profile shown in Fig. 2, where S_{a}, S_{b}, and S_{c} stand for the driving signals of the upper switches in each phase leg, $d_{\mathrm{a\_i}}$, $d_{\mathrm{b\_i}}$, and $d_{\mathrm{c\_i}}$ are the duty cycles of the upper switches in the ith switching period, $\tau_{\mathrm{a\_i}}$, $\tau_{\mathrm{b\_i}}$, and τ_{0_i} are the on-times of the active and zero switching vectors, $v_{\mathrm{dc\_i}}$, $i_{\mathrm{a\_i}}$, $i_{\mathrm{b\_i}}$, and $i_{\mathrm{c\_i}}$ are the measured

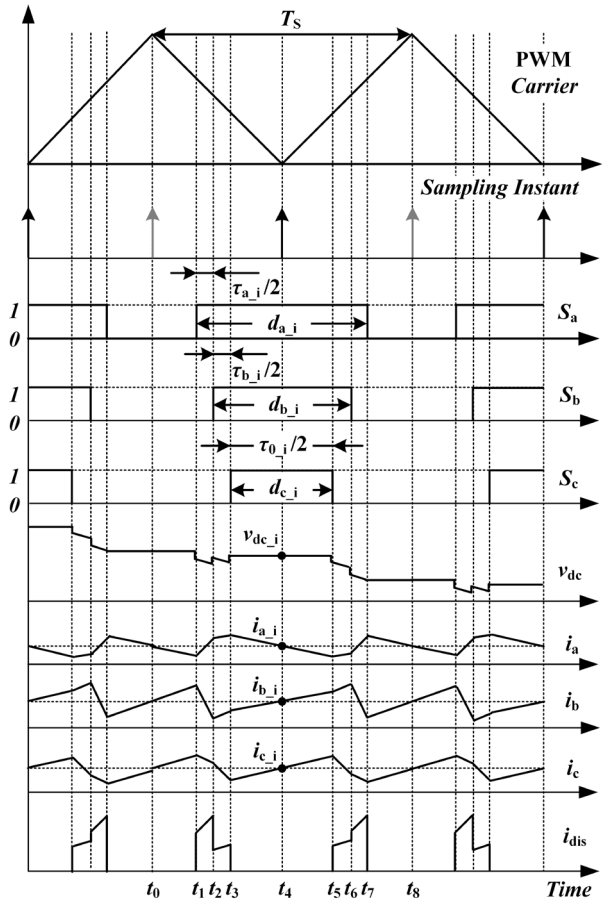

Fig. 3. Key waveforms within the ith switching period of the discharge with the rotor electrical angle θ_{e} of π/12, and the space vector modulator correspondingly operates in the switching sector 1 in steady state. T_{S} is the switching period, S_{a}, S_{b}, and S_{c} are the driving signals of the three-phase upper switches, $d_{\mathrm{a\_i}}$, $d_{\mathrm{b\_i}}$, and $d_{\mathrm{c\_i}}$ are the duty cycles, $\tau_{\mathrm{a\_i}}$, $\tau_{\mathrm{b\_i}}$, and τ_{0_i} are the switching vector on-times, $v_{\mathrm{dc\_i}}$, $i_{\mathrm{a\_i}}$, $i_{\mathrm{b\_i}}$, and $i_{\mathrm{c\_i}}$ are the DC-link voltage and three-phase stator currents measured in the ith switching period.

DC-link voltage and three-phase stator current. Since the DC-link voltage and phase currents are typically measured at the peak or valley of the PWM carrier, where the capacitor discharge current i_{dis} and the voltage drop on the ESR are zero, the measured voltage $v_{\mathrm{dc\_i}}$ is the capacitor voltage. In addition, it can be seen from Fig. 3 that the three-phase stator currents are symmetrical within one switching period. Hence, the measured currents $i_{\mathrm{a\_i}}$, $i_{\mathrm{b\_i}}$, and $i_{\mathrm{c\_i}}$ are the average values of the stator currents over the switching period T_{S}. Combined with the duty cycles $d_{\mathrm{a\_i}}$, $d_{\mathrm{b\_i}}$, and $d_{\mathrm{c\_i}}$ obtained from the controller, the average discharge current $i_{\mathrm{dis\_ave\_Tsi}}$ over the ith switching period can be calculated as

$$i_{dis\_ave\_Tsi} = i_{a\_i} * d_{a\_i} + i_{b\_i} * d_{b\_i} + i_{c\_i} * d_{c\_i} \tag{3}$$

Assuming that the estimation interval Δt includes n switching periods, the average discharge current $i_{\mathrm{dis\_ave}}$ over the entire estimation interval is

$$i_{dis\_ave} = \frac{1}{n}\sum_{i=1}^{n}\left(i_{a\_i} * d_{a\_i} + i_{b\_i} * d_{b\_i} + i_{c\_i} * d_{c\_i}\right) \tag{4}$$

$$C = \frac{i_{dis\_ave}\Delta t}{\Delta v_C} = \frac{(n-1)T_s \sum_{i=1}^{n}\left(i_{a\_i} * d_{a\_i} + i_{b\_i} * d_{b\_i} + i_{c\_i} * d_{c\_i}\right)}{n\left(v_{dc\_1} - v_{dc\_n}\right)} \tag{5}$$

$$i_{dis\_ave} = \frac{1}{n^2}\left(\sum_{i=1}^{n} i_{a\_i} \sum_{i=1}^{n} d_{a\_i} + \sum_{i=1}^{n} i_{b\_i} \sum_{i=1}^{n} d_{b\_i} + \sum_{i=1}^{n} i_{c\_i} \sum_{i=1}^{n} d_{c\_i}\right) \tag{6}$$

$$d_{a/b/c} = \begin{cases} d_{a/b/c\_cal} + \left(t_{d(off)} - t_d - t_{on}\right)/T_s & if\ i_{a/b/c} > 0 \\ d_{a/b/c\_cal} + \left(t_d - t_{off} + t_{d(on)}\right)/T_s & if\ i_{a/b/c} < 0 \end{cases} \tag{7}$$

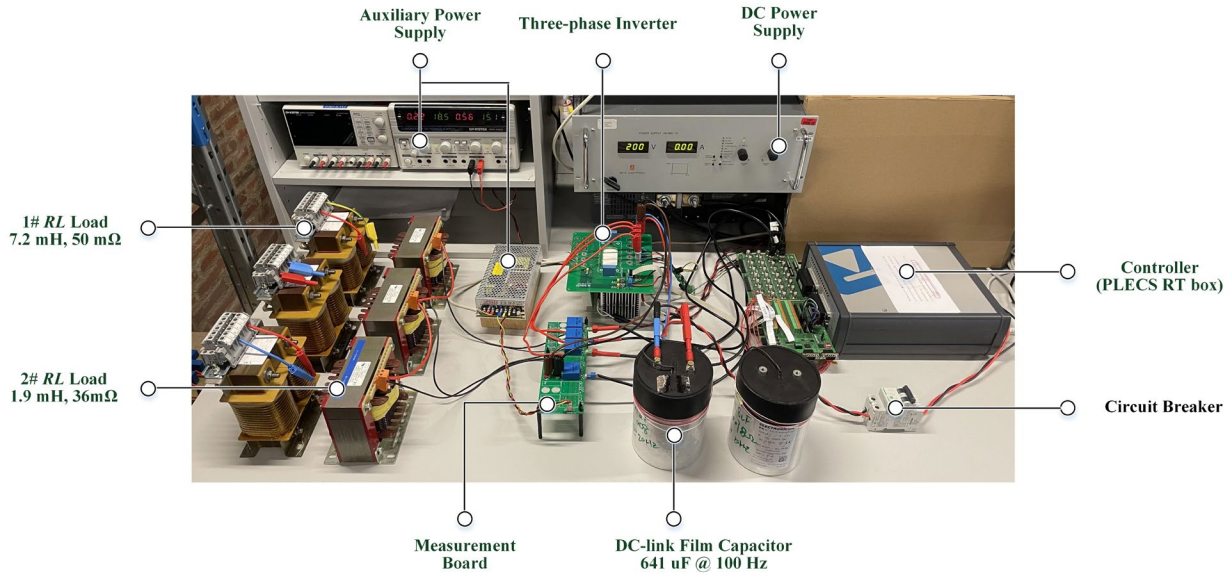

Fig. 5. A down-scaled experimental setup for simulating the DC-link discharge of electric drive systems.

Substituting (4) and the measured DC-link voltage into (2), the capacitance of the DC-link capacitor can be estimated by (5), where all the required data is the existing information in the electric drive system. It is worth stating that the above estimation principle is applicable to arbitrary rotor angles.

IV. Error Analysis and Improvement Solution

In practical applications, errors in the existing information can reduce the estimation accuracy. The error in the DC-link voltage is negligible due to the high capacitor voltage drop over the estimation period, but the errors in the three-phase stator currents and duty cycles cannot be ignored due to the low average discharge current.

The errors in the measured stator currents are generally random and related to the system noises, the accuracy of sensors, and the resolution of analog-to-digital converters. In addition, it can be known from (3) that the stator currents should be sampled with switching frequency at the valley of the PWM carrier to obtain the average stator current during each switching period. However, in practice, the sampling frequency is usually lower than the switching frequency for control purposes only, and asynchronous sampling is typically implemented, i.e., the sampling may occur in the vicinity of the peak or valley of the PWM carrier. These inherent noise and unsatisfactory sampling will eventually lead to considerable errors in the measured current signals.

To reduce the influence of the current errors, the estimation interval is limited to the steady state shown in Fig. 2, and thus the average capacitor discharge current over the steady state can be calculated by averaging the three-phase stator currents and duty cycles, as given in (6). The averaging processing will also attenuate the random errors in the duty cycle, and reduce the sampling requirements for the phase currents as well as the computational effort of the estimation procedure.

In addition to the random error, the bias error in the duty cycle significantly impacts the estimation accuracy, mainly caused by the dead time insertion and non-ideal switching characteristics. It can be known from Fig. 3 and (3) that the duty cycles for estimating the average discharge current should correspond to the time interval during which the upper leg current of each half-bridge circuit is not zero, while the duty cycles obtained from the control system are calculated from the switching vector on-times. In practice, a dead time t_d is always inserted into the driving signals to prevent both upper and lower switches from conducting, and the turn-on and turn-off switching transients of power semiconductor switches are not ideal. It implies that the duty cycles calculated in the control system are not consistent with the actual values. Hence, to guarantee the estimation accuracy, the duty cycles $d_{a/b/c\_cal}$ obtained from the controller must be

compensated with dead time and switching times according to the polarity of corresponding phase currents, as given in (7).

V. Experimental Verification

To verify the feasibility and accuracy of the proposed estimation method, a scaled-down experimental platform is established, as shown in Fig. 5. A film capacitor of ELECTRONICON™ PK16 is used for the DC-link design, and its capacitance value is measured by an LCR meter at 100 Hz. A DC power supply is connected to the DC-link of the three-phase inverter to simulate the battery pack in EVs. The three-phase inverter integrates an IGBT module of Infineon FS25R12KT3 and a gate driver of SEMIKRON SKHI 61, and is mounted on an aluminum heatsink with a cooling fan and a temperature-controlled heating system. The same control strategy as used in the real electric drive system is implemented by a PLECS RT box, and the operating frequency is set at 10 kHz. Constrained by the power capacity of the laboratory, the #1 three-phase *RL* load is used to simulate the motor stator windings.

For the DC-link discharges in real electric drive systems, the main operating variables include the rotor electrical angle θ_e, the initial capacitor voltage V_{C0}, and the equivalent impedance of motor stator windings due to their dependence on current and temperature. In the established experimental platform, the rotor electrical angle θ_e can be set in the controller (i.e., PLECS RT box), and the initial capacitor voltage V_{C0} is controlled by the DC power supply. The variation in the winding impedance is simulated by connecting the #2 *RL* load in series on the load side.

Fig. 6 gives an experimental discharge profile with the discharge command i_{d_ref} of 5 A, rotor electrical position θ_e of $\pi/6$, initial capacitor voltage V_{C0} of 200 V, and #1 *RL* load. It can be seen that the circuit breaker is opened at about 0.04s, and subsequently, the current reference i_{d_ref} is set to 5 A to discharge the capacitor. As the inverter prototype is driven, the DC-link voltage decreases gradually, and the three-phase current reaches a steady state after a short transient and remains constant until the DC-link voltage drops to 45 V.

The DC-link discharges were performed under different operating and environmental conditions, as given in Table I, where each case contains three tests and the discharge current reference i_{d_ref} is always set at 5A. To secure the estimation accuracy, the average discharge current is calculated by averaging the phase current and duty cycle data over the steady state, as given in (6), and the duty cycles are compensated by dead time and switching times with (7).

Fig. 7 summarizes the estimated capacitance from the discharge profiles with a sampling frequency of 1 kHz, where the test cases are represented by different colored markers, and the same colored markers represent the distribution of the estimated results at the same test condition. It can be seen that the estimation results are

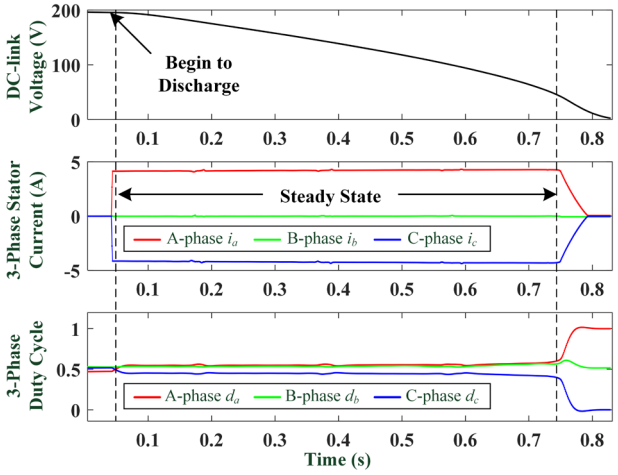

Fig. 6. An experimental discharge profile with the discharge command i_{d_ref} of 5 A, rotor electrical position θ_e of $\pi/6$, initial capacitor voltage V_{C0} of 200 V, and *RL* load of 7.2 mH and 50 mΩ.

Table I. Discharge tests at different operating and environmental conditions

Case	θ_e	V_{C0}	*RL* Load	Discharge Times
1	π*1/6	200 V	7.2 mH, 50 mΩ	3
2	π*3/6	200 V	7.2 mH, 50 mΩ	3
3	π*5/6	200 V	7.2 mH, 50 mΩ	3
4	π*7/6	200 V	7.2 mH, 50 mΩ	3
5	π*9/6	200 V	7.2 mH, 50 mΩ	3
6	π*11/6	200 V	7.2 mH, 50 mΩ	3
7	π*1/6	230 V	7.2 mH, 50 mΩ	3
8	π*1/6	200 V	9.1 mH, 86 mΩ	3

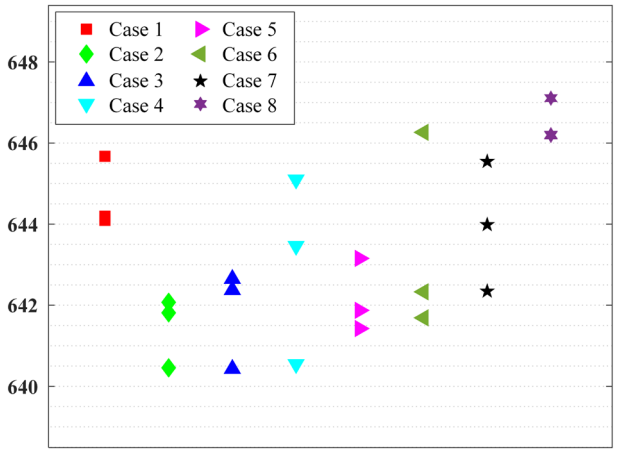

Fig. 7. Estimation results at different test conditions through discharge profiles with a sampling frequency of 1 kHz.

close to the true capacitance value of 641 μF and independent of the changes in rotor electrical angle, initial capacitor voltage, and load impedance. The maximum absolute estimation error is limited to 6.11 μF, which is about 0.95% of the true value. The experimental results indicate that a high estimation accuracy can be achieved at a sampling frequency lower than the switching frequency,

and the resolution for the degradation-induced capacitance change can potentially reach 1% in practice after temperature calibration.

VI. Conclusions

This paper presents a DC-link capacitance estimation method for a three-phase inverter which has the advantages of 1) it is based on existing hardware and software platform; 2) it is non-invasive, implemented during the inverter turning off transition without interfacing its normal operation. Experimental results prove the feasibility and accuracy of the proposed method, with an estimation error of less than 0.95 % at moderate requirements on sampling frequency and sensor accuracy. The authors consider it as a promising method for Electric Vehicle (EV) applications without additional cost and new risk introduced to existing traction inverter systems.

References

[1] H. Wang and F. Blaabjerg, "Reliability of capacitors for dc-link applications in power electronic converters—an overview," *IEEE Trans. Ind. Appl.*, vol. 50, no. 5, pp. 3569–3578, 2014.

[2] H. Wang, H. Wang, G. Zhu, and F. Blaabjerg, "An overview of capacitive dc-links-topology derivation and scalability analysis," *IEEE Trans. Power Electron.*, vol. 35, no. 2, pp. 1805–1829, 2019.

[3] H. Wen, W. Xiao, X. Wen, and P. Armstrong, "Analysis and evaluation of dc-link capacitors for high-power-density electric vehicle drive systems," *IEEE Trans. Veh. Technol.*, vol. 61, no. 7, pp. 2950– 2964, 2012

[4] H. Wang, P. Davari, H. Wang, D. Kumar, F. Zare, and F. Blaabjerg, "Lifetime estimation of dc-link capacitors in adjustable speed drives under grid voltage unbalances," *IEEE Trans. Power Electron.*, vol. 34, no. 5, pp. 4064–4078, 2018.

[5] J. Falck, C. Felgemacher, A. Rojko, M. Liserre, and P. Zacharias, "Reliability of power electronic systems: An industry perspective," *IEEE Ind. Electron. Mag*., vol. 12, no. 2, pp. 24–35, 2018.

[6] F. Blaabjerg, H. Wang, I. Vernica, B. Liu, and P. Davari, "Reliability of power electronic systems for ev/hev applications," *Proceedings of the IEEE*, vol. 109, no. 6, pp. 1060–1076, 2020.

[7] H. Wang, M. Liserre, and F. Blaabjerg, "Toward reliable power electronics: Challenges, design tools, and opportunities," *IEEE Ind. Electron. Mag*., vol. 7, no. 2, pp. 17–26, 2013.

[8] S. Yang, D. Xiang, A. Bryant, P. Mawby, L. Ran, and P. Tavner, "Condition monitoring for device reliability in power electronic converters: A review," *IEEE Trans. Power Electron.*, vol. 25, no. 11, pp. 2734–2752, 2010.

[9] S. Yang, A. Bryant, P. Mawby, D. Xiang, L. Ran, and P. Tavner, "An industry-based survey of reliability in power electronic converters," *IEEE Trans. Ind. Appl.*, vol. 47, no. 3, pp. 1441–1451, 2011.

[10] A. Gupta, O. P.Yadav, D. DeVoto, and J. Major, "A review of degradation behavior and modeling of capacitors," in *Proc. Int. Tech. Conf. Exhib. Packag. Integr. Electron. Photon. Microsyst*., Oct. 2018, pp. 1–10.

[11] A. Shrivastava, M. H. Azarian, C. Morillo, B. Sood, and M. Pecht, "Detection and reliability risks of counterfeit electrolytic capacitors," *IEEE Trans. Rel.*, vol. 63, no. 2, pp. 468–479, Jun. 2014.

[12] C. Andersson, J. Ingman, E. Varescon, and M. Kiviniemi, "Detection of cracks in multilayer ceramic capacitors by X-ray imaging," *Microelectron. Rel.*, vol. 64, pp. 352–356, 2016.

[13] C. Andersson, O. Kristensen, S. Miller, T.Gloor, and F. Iannuzzo, "Lockin thermography failure detection on multilayer ceramic capacitors after flex cracking and temperature–humidity–bias stress," *IEEE J. Emerg. Sel. Top. Power Electron.*, vol. 6, no. 4, pp. 2254–2261, Dec. 2018.

[14] H. Wang, R. Zhu, H. Wang, M. Liserre, and F. Blaabjerg, "A thermal modeling method considering ambient temperature dynamics," *IEEE Trans. Power Electron.*, vol. 35, no. 1, pp. 6–9, Jan. 2020.

[15] Z. Zhao, P. Davari, W. Lu, H. Wang, and F. Blaabjerg, "An overview of condition monitoring techniques for capacitors in dc-link applications," *IEEE Trans. Power Electron.*, vol. 36, no. 4, pp. 3692–3716, 2020.

[16] W. Lu, X. Lu, J. Han, Z. Zhao, and X. Du, "Online estimation of esr for dc-link capacitor of boost pfc converter using wavelet transform based time–frequency analysis method," *IEEE Trans. Power Electron.*, vol. 35, no. 8, pp. 7755–7764, 2019.

[17] P. Sundararajan et al., "Condition monitoring of dc-link capacitors using goertzel algorithm for failure precursor parameter and temperature estimation," *IEEE Trans. Power Electron.*, vol. 35, no. 6, pp. 6386–6396, Jun. 2020.

[18] M. Makdessi, A. Sari, G. Aubard, P. Venet, C. Joubert, and J. Duwattez, "Online health monitoring of metallized polymer film capacitors for avionics applications," in *Proc. IEEE 24th Int. Symp. Ind. Electron.*, Jun. 2015, pp. 1296–1301.

[19] D. C. Lee, K. J. Lee, J. K. Seok, and J. W. Choi, "Online capacitance estimation of DC-link electrolytic capacitors for three-phase AC/DC/AC PWM converters using recursive least squares method," *IEE Proc.-Elect. Power Appl.*, vol. 152, no. 6, pp. 1503–1508, Nov. 2005.

[20] X. S. Pu, T. H. Nguyen, D. C. Lee, K. B. Lee, and J. M. Kim, "Fault diagnosis of DC-link capacitors in three-phase AC/DC PWM converters by online estimation of equivalent series resistance," *IEEE Trans. Ind. Electron.*, vol. 60, no. 9, pp. 4118–4127, Sep. 2013.

[21] A. G. Abo-Khalil and D. C. Lee, "DC-link capacitance estimation in AC/DC/AC PWM converters using voltage injection," *IEEE Trans. Ind. Appl.*, vol. 44, no. 5, pp. 1631–1637, Sep./Oct. 2008.

[22] X. Pu, T. H. Nguyen, D. C. Lee, and S. G. Lee, "Capacitance estimation of DC-link capacitors for single-phase PWM converters," in *Proc. IEEE 6th Int. Power Electron. Motion Control Conf*., 2009, pp. 1656–1661.

[23] T. H. Nguyen and D. C. Lee, "Deterioration monitoring of DC-link capacitors in AC machine drives by current injection," *IEEE Trans. Power Electron*., vol. 30, no. 3, pp. 1126–1130, Mar. 2015.

[24] S. Lee et al., "A new strategy for condition monitoring of adjustable speed induction machine drive systems," *IEEE Trans. Power Electron*., vol. 26, no. 2, pp. 389–398, Feb. 2011.

[25] Y. Yu, T. Zhou, M. Zhu, and D. Xu, "Fault diagnosis and life prediction of DC-link aluminum electrolytic capacitors used in three-phase AC/DC/AC converters," in *Proc. 22nd Int. Conf. Instrum., Meas., Comput., Commun. Control*, Harbin, China, 2012, pp. 825–830.

[26] K.-W. Lee, M. Kim, J. Yoon, S. B. Lee, and J.-Y. Yoo, "Condition monitoring of DC-link electrolytic capacitors in adjustable-speed drives," *IEEE Trans. Ind. Appl*., vol. 44, no. 5, pp. 1606–1613, Sep./Oct. 2008.

[27] H. Li, D. Xiang, X. Han, X. Zhong, and X. Yang, "High-accuracy capacitance monitoring of dc-link capacitor in VSI systems by LC resonance," *IEEE Trans. Power Electron*., vol. 34, no. 12, pp. 12200–12211, Dec. 2019.

[28] Y. Wu and X. Du, "A VEN condition monitoring method of DC-link capacitors for power converters," *IEEE Trans. Ind. Electron*., vol. 66, no. 2, pp. 1296–1306, Feb. 2019.

[29] M. Kim, S. Sull, and J. Lee, "Condition monitoring of dc-link capacitors in drive system for electric vehicles," in *Proc. IEEE Veh. Power Propulsion Conf*., Seoul, South Korea, Oct. 9–12, 2012, pp. 633–637.

[30] J. Reimers, L. Dorn-Gomba, C. Mak, and A. Emadi, "Automotive traction inverters: Current status and future trends," *IEEE Trans. Veh. Technol*., vol. 68, no. 4, pp. 3337–3350, Apr. 2019.